SCIENTIFIC REPORTS

OPEN

# Trends in $(LaMnO_3)_n/(SrTiO_3)_m$ superlattices with varying layer thicknesses

Received: 04 March 2015
Accepted: 04 August 2015
Published: 01 September 2015

J. Jilili, F. Cossu & U. Schwingenschlögl

**We investigate the thickness dependence of the structural, electronic, and magnetic properties of $(LaMnO_3)_n/(SrTiO_3)_m$ ($n$, $m = 2$, 4, 6, 8) superlattices using density functional theory. The electronic structure turns out to be highly sensitive to the onsite Coulomb interaction. In contrast to bulk $SrTiO_3$, strongly distorted O octahedra are observed in the $SrTiO_3$ layers with a systematic off centering of the Ti atoms. The systems favour ferromagnetic spin ordering rather than the antiferromagnetic spin ordering of bulk $LaMnO_3$ and all show half-metallicity, while a systematic reduction of the minority spin band gaps as a function of the $LaMnO_3$ and $SrTiO_3$ layer thicknesses originates from modifications of the Ti $d_{xy}$ states.**

A zoo of extraordinary phenomena, such as two dimensional quantum gases[1], superconductivity[2], magnetism[3], magnetoresistance[4], exchange bias[5,6], half-metallicity[7], and ferroelectricity[8], is hosted by perovskite oxide heterostructures. The lattice, charge, orbital, and spin degrees of freedom and their competition give rise to these properties[9]. In general, electrostatic and strain effects drive structural and electronic reconstructions at interfaces[10], which thus often behave distinctly different from their component materials. Nowadays the thickness of superlattices can be determined and controlled down to the atomic scale, where interface effects become more and more important. Thus, the thickness is a key factor for tailoring the electronic and transport properties. For example, Nanda and coworkers[11] have studied the magnetism in $LaMnO_3/SrMnO_3$ superlattices with varying layer thicknesses, concluding that the charge reconstruction is confined to two unit cells around the interfaces. Volume changes have been observed in $NaNbO_3/SrTiO_3$ superlattices[12], for example, and it has been demonstrated that the appearance of metallicity correlates with the layer thicknesses[13].

Manganites and titanates are popular perovskite oxides, displaying colossal magnetoresistance[14] and superconductivity[15]. Colossal magnetoresistance was first observed in 1994 in $La_{1-x}Ca_xMnO_3$[16] and gained considerable attention thereafter. The parent compound, $LaMnO_3$, is an antiferromagnetic insulator, which becomes ferromagnetic under hole doping with Ca[17], Sr[18], and Ba[19]. Therefore, superlattices with $SrTiO_3$ can be expected to show an unusual magnetic behavior and accordingly are attracting interest both for fundamental and technological reasons. The authors of Ref. 20, for example, have reported significant doping effects in $LaMnO_3/SrTiO_3$ superlattices, which can extend over few unit cells[21], and have studied their origin. In $LaSrMnO_3/SrTiO_3$ superlattices with $SrTiO_3$ layers thinner than 1 nm an interfacial charge transfer leads to finite Ti magnetic moments[22]. In general, the thicknesses of the component layers in a $LaMnO_3/SrTiO_3$ superlattice seem to strongly influence the magnetic and transport properties[23]. This would be interesting, because the behavior of the system could be controlled by means of the layer thickness. However, it requires detailed understanding of the strong lattice distortions and their implications for the physics of this superlattice, which is the topic of the present study.

## Results

$(LaMnO_3)_n/(SrTiO_3)_m$ superlattices are modeled by a $\sqrt{2} \times \sqrt{2}$ in-plane supercell of the cubic perovskite structure for taking into account possible effects of octahedral rotations. We use the Vienna Ab-initio

KAUST, PSE Division, Thuwal 23955-6900, Kingdom of Saudi Arabia. Correspondence and requests for materials should be addressed to U.S. (email: udo.schwingenschlogl@kaust.edu.sa)

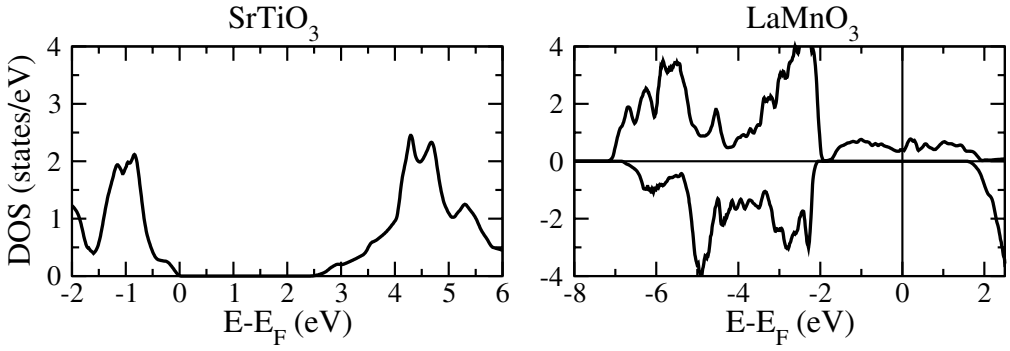


**Figure 1. Total densities of states of bulk $SrTiO_3$ and strained bulk $LaMnO_3$.**

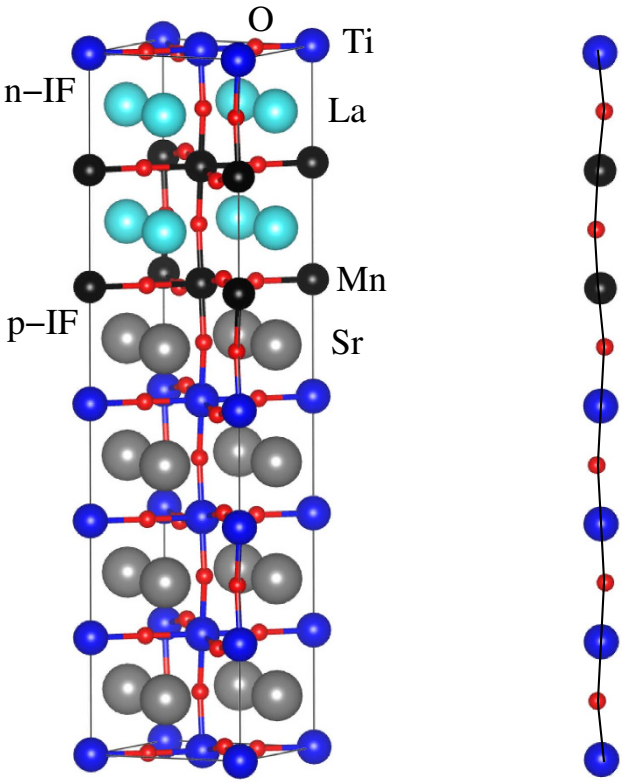


**Figure 2.** Left: Structure of the $(LaMnO_3)_n/(SrTiO_3)_m$ superlattice for $n{:}m = 2{:}4$. Right: Schematic view of the Mn-O and Ti-O bonds perpendicular to the interfaces.

Simulation Package[24] with projector augmented wave pseudopotentials and employ the generalized gradient approximation in the parametrization of Perdew, Burke, and Ernzerhof (including spin polarization). The density of states is calculated by the tetrahedron method (smearing 0.01 eV) with Blöchl corrections[25]. Because of the correlated nature of the transition metal *d* orbitals, we add an onsite Coulomb interaction using the Lichtenstein scheme[26]. The values for the *U* and *J* parameters are taken from Refs 27–29 as 4 eV and 1 eV for the Mn *d* states, 5 eV and 0.5 eV for the Ti *d* states, and 9 eV and 1 eV for the La *f* states. We have tested for the bulk compounds that these values are transferable to the parametrization of Perdew, Burke, and Ernzerhof by comparing the densities of states, which show no qualitative difference. The optimized lattice constant of $SrTiO_3$ is 3.97 Å, with a band gap of 2.6 eV, and the optimized in-plane and out-of-plane lattice constants of $LaMnO_3$ are 3.95 Å and 4.01 Å. The total densities of states obtained for bulk $SrTiO_3$ and strained bulk $LaMnO_3$ (half-metallic) are shown in Fig. 1.

| | | *n*-IF | *p*-IF | | *n*-IF | *p*-IF |
|---|---|---|---|---|---|---|
| Mn-O | 2:2 | 2.12 | 2.13 | 4:4 | 2.17 | 2.00 |
| Ti-O | | 2.04 | 1.91 | | 2.01 | 1.90 |
| Mn-O | 2:4 | 2.17 | 2.03 | 4:2 | 2.14 | 2.07 |
| Ti-O | | 2.00 | 1.93 | | 2.04 | 1.88 |
| Mn-O | 2:6 | 2.12 | 2.01 | 6:2 | 2.14 | 2.07 |
| Ti-O | | 1.95 | 1.96 | | 2.04 | 1.91 |
| Mn-O | 2:8 | 2.12 | 1.99 | 8:2 | 2.13 | 2.13 |
| Ti-O | | 1.95 | 1.97 | | 2.08 | 1.87 |

**Table 1. Bond distances (in Å) at the n-IF and p-IF for different *n*:*m*.**

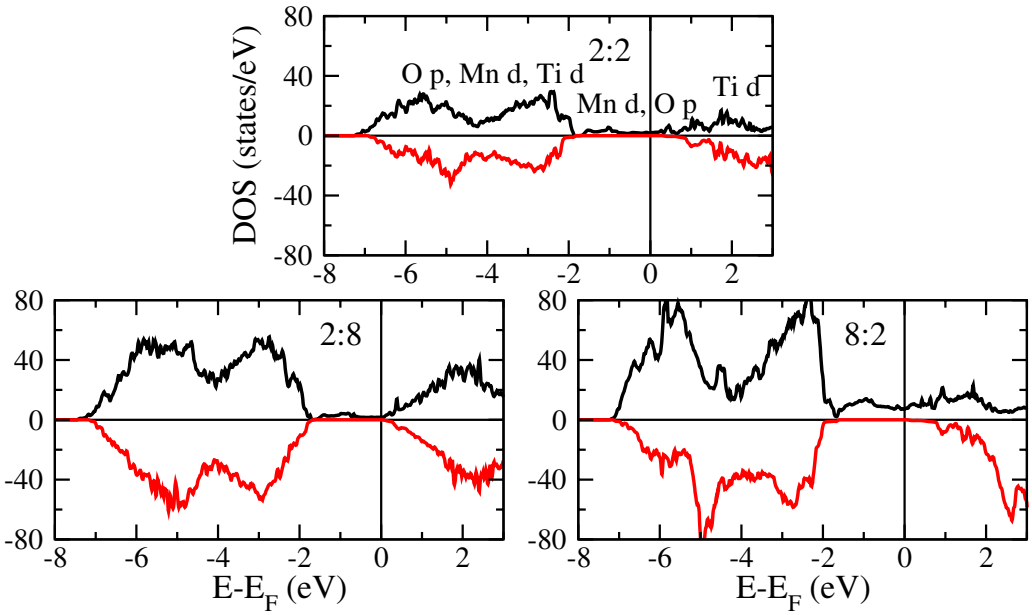


**Figure 3. Total densities of states for thicknesses n:m = 2:2, 2:8, and 8:2.**

Structural optimization of the superlattices with and without onsite interaction is found to yield substantial differences in the electronic structure, especially near the Fermi level. More specifically, the minority channel shows a metallic character without onsite interaction for $n{:}m = 2{:}2$ (2 unit cells of $LaMnO_3$ alternate with 2 unit cells of $SrTiO_3$), whereas with onsite interaction we obtain a half-metallic character. The supercells have $C_{2h}$ point group symmetry (tetragonal perovskite structure). An optimized in-plane lattice constant of 5.56 Å is obtained for the 2:2 system and is used for the larger superlattices. The out-of-plane lattice constant is optimized individually in each case. Starting from the 2:2 system, we fix the $LaMnO_3$ thickness and increase the $SrTiO_3$ thickness (2:4, 2:6, 2:8) or fix the $SrTiO_3$ thickness and increase the $LaMnO_3$ thickness (4:2, 6:2, 8:2). The 4:4 system is also considered for comparison. Figure 2(left) illustrates the 2:4 system as an example. There are two types of interfaces, the *n*-type LaO/$TiO_2$ interface and the *p*-type SrO/$MnO^2$ interface, denoted in the following as n-IF and p-IF, respectively. The nomenclature refers to the compensating charges formed at the $(La^{3+}O^{2-})^{+}/(Ti^{4+}O_2^{2-})^{0}$ and $(Sr^{2+}O^{2-})^{0}/(Mn^{3+}O_2^{2-})^{-}$ contacts, respectively.

The Ti-O-Mn bond angle at the n-IF (where the $MnO_6$ and $TiO_6$ octahedra are connected) is found to be 159.4°, whereas at the p-IF it has a larger value of 164.8°, which corresponds to a reduced tilting. While substantial modifications of the structure are expected in the vicinity of an interface, strong effects are also observed for the O octahedra further apart. For instance, the Mn-O-Mn bond angles increase by up to 8.3° with respect to the bulk value (154.6°), which supports double exchange. On the other hand, the Ti-O-Ti bond angles strongly decrease throughout the $SrTiO_3$ layer, reflecting huge distortions as compared to the bulk cubic structure. In general, the Ti-O-Ti (Mn-O-Mn) bond angles near the p-IF (n-IF) are less modified, because the distance to the interface is larger. The tiltings of the O octahedra are found to vary distinctly for different thicknesses *n*:*m*, and so do the electronic properties.

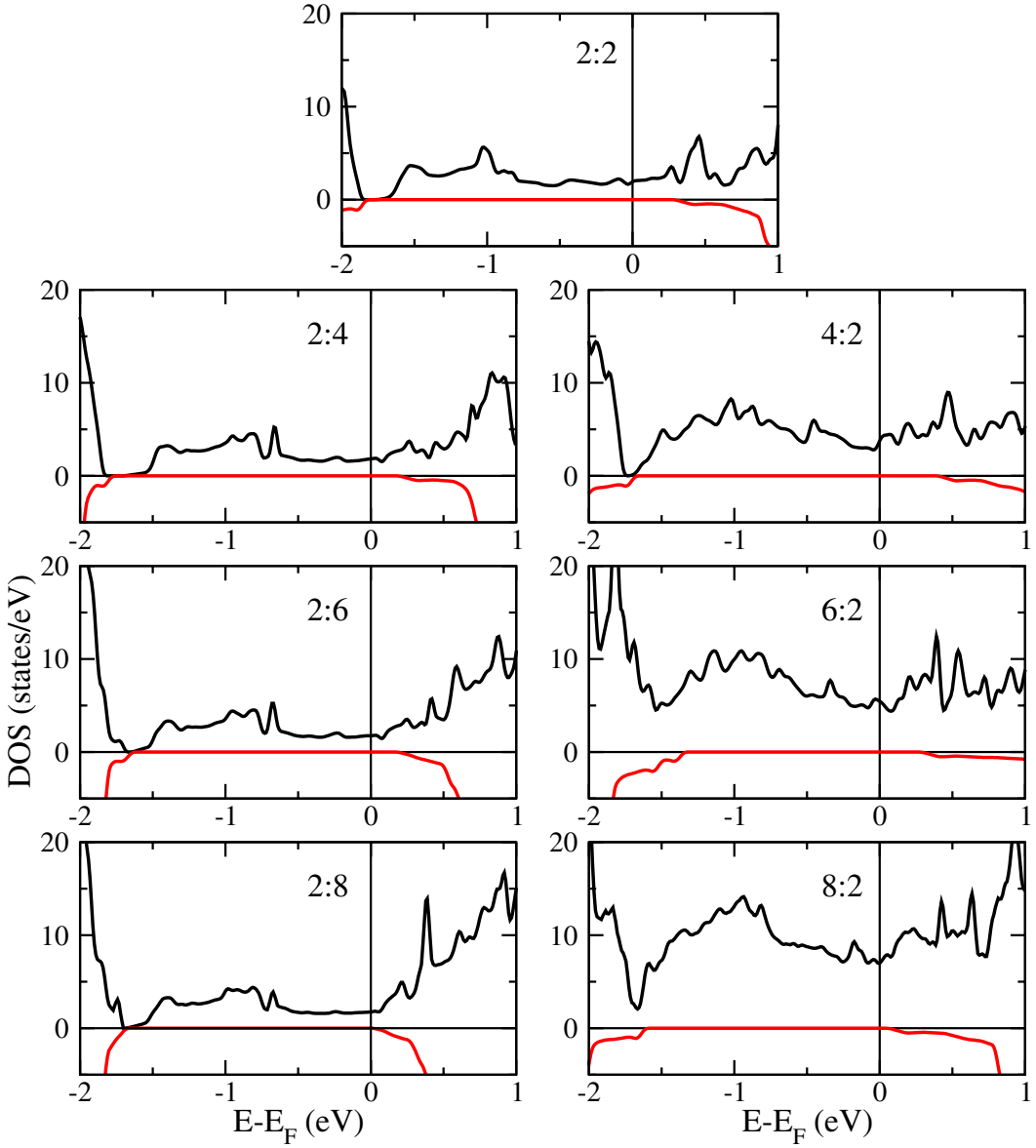


**Figure 4. Total densities of states near the Fermi energy for thicknesses *n*:*m* = 2:2, 2:4, 2:6, 2:8, 4:2, 6:2, and 8:2.**

For increasing *m* the Mn-O (Ti-O) bond length along the *z* axis at the p-IF decreases (increases) from 2.13 Å to 1.99 Å (1.91 Å to 1.97 Å), while at the n-IF the Mn-O bond length stays close to 2.13 Å and the Ti-O bond length decreases from 2.04 Å to 1.95 Å, see Table 1. A schematic view of the Mn-O and Ti-O bonds is given in Fig. 2(right). For increasing *n* the Mn-O bond length at the p-IF maintains a value of 2.10 Å, while the Ti-O bond length decreases (bulk value 1.95 Å) from 1.91 Å in the 2:2 system to 1.87 Å in the 8:2 system. At the n-IF the Mn-O bond length shows no clear trend, while the Ti-O bond length grows significantly from 2.04 Å in the 2:2 system to 2.08 Å in the 8:2 system. It is found that all Ti atoms shift systematically off the center of their O octahedron towards the p-IF by up to 0.1 Å (in all cases more at the p-IF than at the n-IF), implying that a permanent dipole is created, while bulk $SrTiO_3$ is not ferroelectric. The off-centering is generally enhanced at the interfaces when *n* increases and reduced when *m* increases. It is known that the properties of $SrTiO_3$ are very sensitive to dopants and external perturbations[30] so that it cannot surprise that the superlattices react similarly[31]. We also note that we obtain for bulk $SrTiO_3$ a ferroelectric distortion of 0.03 Å, which is a known artefact of the employed methodology[32]. However, this effect is significantly smaller than the off-centerings described above and therefore does not affect our conclusions.

Bulk $LaMnO_3$ is an A-type antiferromagnetic (AFM) Mott insulator, due to a combination of super-exchange and Zener double exchange[33], whereas $SrTiO_3$ is a non-magnetic insulator ($d^0$ configuration of Ti). Figure 3 shows the total densities of states obtained for the 2:2, 2:8, and 8:2 systems. The general

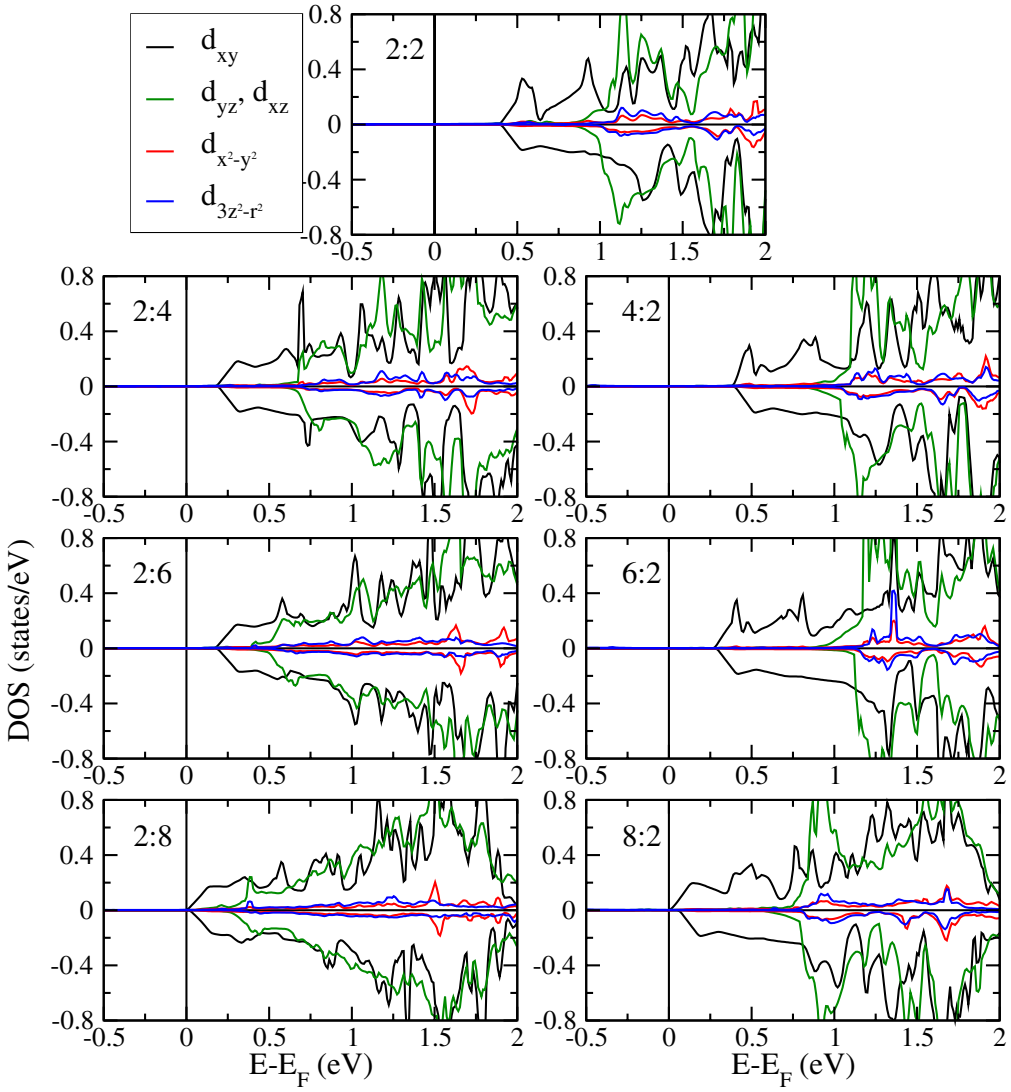


**Figure 5. Projected densities of states of the Ti atom next to the n-IF for thicknesses *n*:*m* = 2:2, 2:4, 2:6, 2:8, 4:2, 6:2, and 8:2.**

shape of the curves is similar, showing half-metallicity in each case. From −7 to −2 eV we find mainly Mn *d*, Ti *d*, and O *p* states, from −2 to 2 eV Mn *d* and O *p* states, and above 2 eV Ti *d*, La *f*, Sr *d*, and O *p* states. Figure 4 demonstrates systematic changes for varying *n* and *m*. The density of states at the Fermi energy remains similar for growing *m* but increases significantly for growing *n* due to the fact that these states mainly belong to the $LaMnO_3$ layer. Importantly, for increasing *n* as well as *m*, the minority spin band gap is reduced substantially. Indeed, the band onsets in the 2:8 and 8:2 systems are close to the Fermi energy so that the half-metallicity will most likely vanish for *n*, *m* > 8.

The reduction of the minority spin band gap is explained by the projected densities of states of the Ti atoms at the n-IF in Fig. 5. The Ti 3*d* orbitals, being split into $d_{xy}$, $d_{yz}$, $d_{xz}$ ($t_{2g}$) and $d_{x^2-y^2}$, $d_{3z^2-r^2}$ ($e_g$) states due to the octahedral crystal field, systematically shift to lower energy for increasing *n* and *m*, which is consistent with previous experimental observations for $LaAlO_3/SrTiO_3$ interfaces[34]. The energetic lowering is strongest for the $d_{xy}$ states, which thus govern the reduction of the minority spin band gap. The orbital ordering seen in Fig. 5 decreases for increasing *m*, while it remains similar for increasing *n*. In addition, it is always more pronounced at the n-IF than at the p-IF, and almost lost at the p-IF and in the bulk-like regions of the 2:8 system. Figure 6 gives projected densities of states of Ti atoms in layers with increasing distance from the 2:8 n-IF. As to be expected, away from the n-IF the states shift to higher energy. Projected densities of states of the Mn atoms at the p-IF are shown in Fig. 7. Note that the Mn $d_{x^2-y^2}$ and $d_{3z^2-r^2}$ orbitals contribute at the Fermi energy in the majority spin channel, though differently for the different systems. Since bulk $LaMnO_3$ forced into $C_{2h}$ symmetry becomes metallic, the conducting

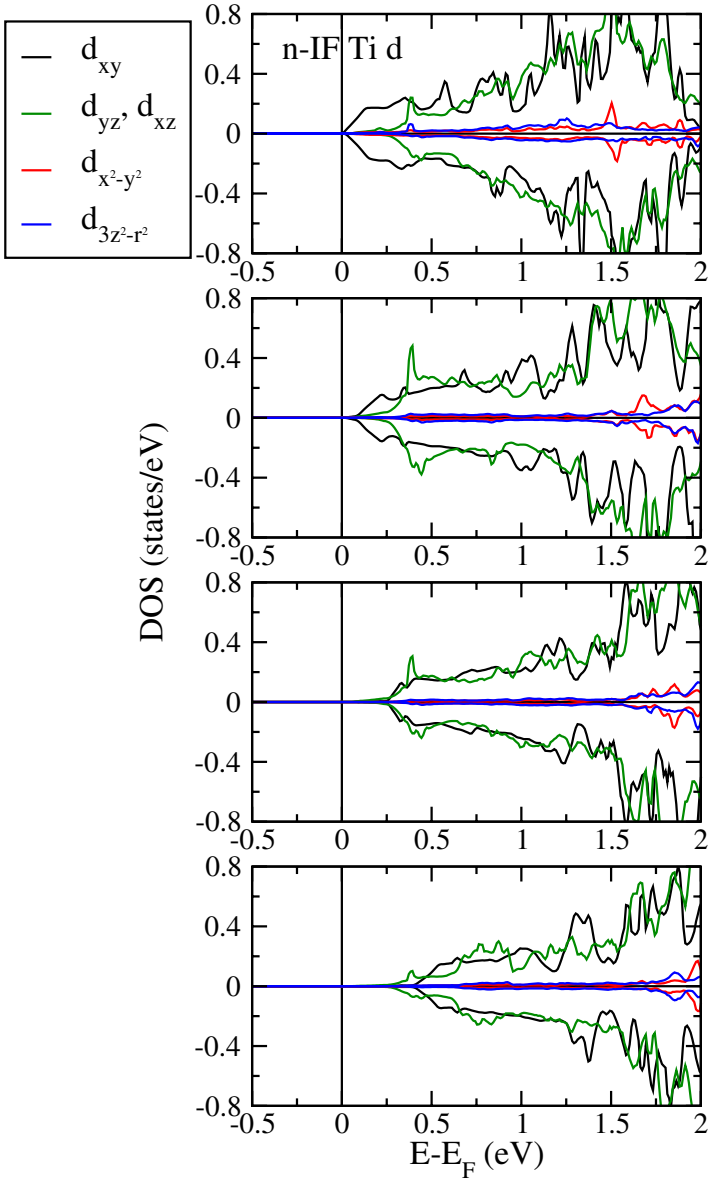


**Figure 6. Projected densities of states of the Ti atoms in layers with increasing distance from the 2:8 n-IF.**

Mn states are a result of the in-plane strain. The metallicity at the p-IF is substantially reduced for increasing $n$, especially in the 8:2 system, as the $LaMnO_3$ layer becomes more bulk-like. Figure 8 gives projected densities of states of the Mn atoms in layers with increasing distance from the 8:2 p-IF. The distinct difference between the $d_{x^2-y^2}$ and $d_{3z^2-r^2}$ states is reduced when the distance increases.

In order to assess the magnetic ground state, we study the total energies for FM and A-type AFM spin ordering for strained bulk $LaMnO_3$ and the superlattices. Other spin orderings (such as C-type and G-type AFM) have much higher energies, as we have checked for the 2:2 system. FM spin ordering is found to be favorable, in agreement with previous experiments[20,23,34] and calculations[35] as well as reports on related perovskite oxide interfaces[36–38]. The energy difference (per formula unit) between FM and A-type AFM spin ordering is 0.75 eV for strained bulk $LaMnO_3$, whereas in the case of the superlattices it slightly decreases from 0.27 eV to 0.20 eV for increasing $m$ and remarkably increases from 0.27 eV to 0.85 eV for increasing $n$, which shows that it can be attributed to the $LaMnO^3$ layer (the Ti magnetic moments are very small). Because of this, we normalize our results in the following with respect to the number of Mn atoms. The energy difference steadily decreases for increasing $n$ as well as $m$ though the FM ordering, which is due to Zener double exchange between partially filled Mn $e_g$ states[39], remains favorable. For $x = 0.3$ FM spin ordering is also established in $La_{1-x}Ca_xMnO_3$, see the neutron diffraction experiments in Ref. 40. Moreover, X-ray magnetic circular dichroism and absorption spectroscopy on

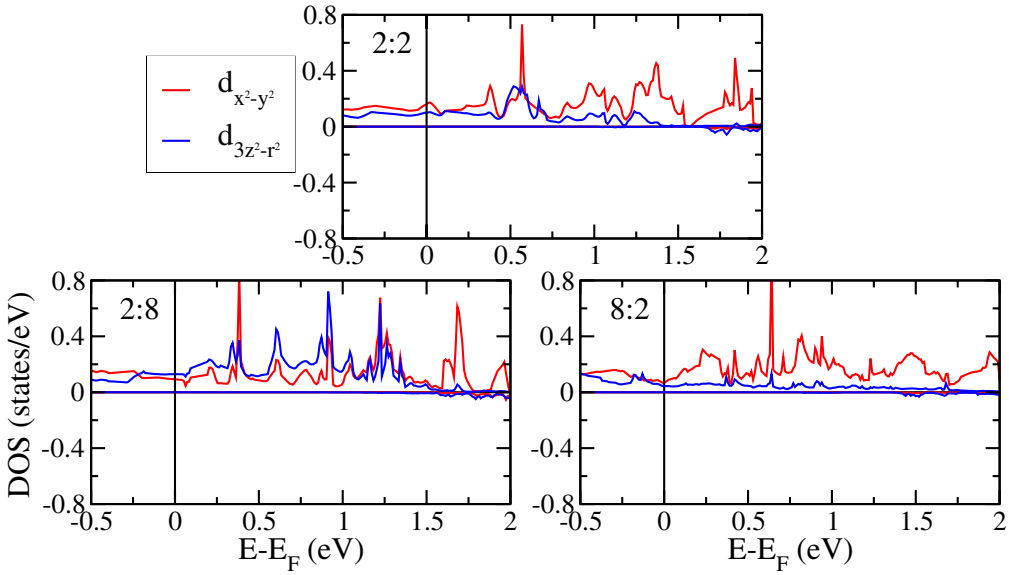


**Figure 7. Projected densities of states of the Mn atom next to the p-IF for thicknesses *n*:*m* = 2:2, 2:8, and 8:2.**

$LaAlO_3/SrTiO_3$ have given direct evidence of a FM interface state, originating from the Ti $d_{xy}$ orbitals[34]. Interestingly, induced Ti magnetic moments of 0.02 to 0.04 $\mu_B$ are observed at both interfaces in our systems, see Table 2, whereas far from the interfaces they are negligible ($<0.01\,\mu_B$). For increasing $m$ they increase (decrease) at the n-IF (p-IF), while for increasing $n$ we obtain higher magnetic moments at the p-IF (~0.04 $\mu_B$) than at the n-IF (~0.02 $\mu_B$). We note that even small Ti magnetic moments at perovskite oxide interfaces can have important consequences for the magnetism[34,41].

We find Mn magnetic moments of 3.72 to 4.03 $\mu_B$, with larger values at the n-IF than at the p-IF in all cases. When $m$ increases they increase (decrease) at the n-IF (p-IF), while the changes are not systematic under variation of $n$. The highest value appears in the 4:4 system at the n-IF. Concerning the charges in the atomic orbitals, we find small but finite differences from the corresponding bulk values at both interfaces, see Table 2. A detailed analysis shows that for increasing $n$ ($m$) the Mn atoms lose more (less) charge at the p-IF. Moreover, the Ti (Mn) atoms gain (lose) charge at the n-IF (p-IF) in all cases, while there is no clear trend at the p-IF (n-IF) because of the larger distances of the atoms from to the interface plane. The observed small charge transfers give rise to the mentioned Ti magnetic moments but cannot explain the ferroelectric distortions in the $SrTiO_3$ layer, which thus are likely direct consequences of the interface interaction.

## Discussion

The structural, electronic, and magnetic properties of $(LaMnO_3)_n/(SrTiO_3)_m$ superlattices have been investigated and compared for various thicknesses *n*:*m*. Both $n$ and $m$ are found to strongly affect the material properties. In general, the $SrTiO_3$ layers show heavy distortions of the O octahedra, which are not present in bulk $SrTiO_3$, consistent with recent experimental findings[42]. Since $LaMnO_3$ is polar along the [001] direction (with alternating $(LaO)^+$ and $(MnO_2)^-$ layers) and $SrTiO_3$ is non-polar, a compensation mechanism is required. As the strained $LaMnO_3$ is metallic, we could expect accumulation of charge carriers at the interfaces. However, this effect is much too small according to the charge deviations reported in Table 2 so that a second mechanism must play a role. The projected densities of states of the Ti atoms in layers of increasing distance from the 2:8 n-IF in Fig. 6 show an almost continuous shift of all curves to higher energy. This reflects the built up of an electric field, which in turn induces ferroelectric distortions in the $SrTiO_3$ region, as discussed before. The ferroelectric distortions constitute the main compensation mechanism in the present superlattice. Similar distortions of the $TiO_6$ octahedra have been reported in Ref. 28.

All studied systems exhibit half-metallicity, though our results indicate that this property will vanish for $n$, $m > 8$. FM spin ordering is always energetically favorable over AFM spin ordering but the preference becomes smaller for increasing $n$, since the A-type AFM ordering of bulk $LaMnO_3$ starts to dominate. The Ti magnetic moments observed at the interfaces are small. The authors of Ref. 43 have found ferromagnetic and antiferromagnetic alignment of the Mn and Ti spins for *n*:*m* ratios of 3:2 and 17:2, respectively, and have argued that Mn-O-Ti superexchange therefore must play a role. In general, defects and cation intermixing are important for the stabilization of perovskite superlattices. For instance,

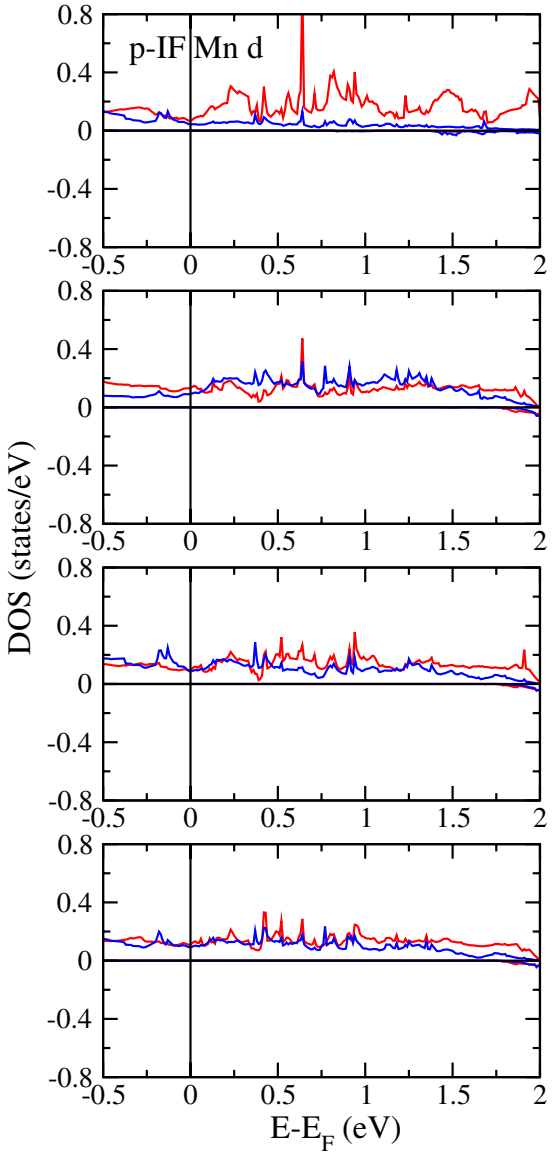


**Figure 8. Projected densities of states of the Mn atoms in layers with increasing distance from the 8:2 p-IF.**

| *n*:*m* | magnetic moment | | | | charge deviation | | | |
|---|---|---|---|---|---|---|---|---|
| | Mn *n*-IF | Mn *p*-IF | Ti *n*-IF | Ti *p*-IF | Mn *n*-IF | Mn *p*-IF | Ti *n*-IF | Ti *p*-IF |
| 2:2 | 3.87 | 3.86 | 0.01 | 0.03 | +0.01 | −0.05 | +0.02 | +0.01 |
| 2:4 | 3.95 | 3.76 | 0.02 | 0.02 | +0.03 | −0.02 | +0.02 | +0.01 |
| 2:6 | 3.96 | 3.74 | 0.02 | 0.02 | +0.03 | −0.02 | +0.02 | +0.01 |
| 2:8 | 3.97 | 3.72 | 0.03 | 0.02 | +0.04 | −0.01 | +0.02 | −0.01 |
| 4:4 | 4.03 | 3.78 | 0.02 | 0.03 | +0.03 | −0.04 | +0.02 | 0.00 |
| 4:2 | 3.99 | 3.85 | 0.02 | 0.03 | 0.00 | −0.04 | +0.01 | +0.01 |
| 6:2 | 4.01 | 3.88 | 0.02 | 0.03 | −0.01 | −0.07 | +0.06 | −0.03 |
| 8:2 | 3.97 | 3.89 | 0.02 | 0.04 | +0.01 | −0.07 | +0.04 | +0.03 |

**Table 2. Magnetic moments (in $\mu_B$) and charge deviations with respect to the bulk (in electrons) of the interfacial Mn and Ti atoms for different *n*:*m*.** Positive (negative) values represent gain (loss) of charge.

the high electrical conductivity of the $LaAlO_3/SrTiO_3$ interface is related to the formation of O vacancies during the deposition process due to the extra charges introduced into the system[44]. In addition, Sr/La intermixing leads to a metallic interface between the insulators $LaTiO_3$ and $SrTiO_3$, because mixed valent Ti states are created[45]. We expect that these factors are less important for the $LaMnO_3/SrTiO_3$ interface, as it was found to be rather sharp[42]. We find a systematic reduction of the minority spin band gaps with increasing $n$ and $m$, which originates mainly from an energetic downshift of the Ti $d_{xy}$ states.

## Methods

The atomic sphere radii are chosen such that overlap is avoided during the ionic relaxation, for which we set the energy tolerance to $10^{-3}$ eV, employ a $4 \times 4 \times 1$ k-mesh, a Gaussian smearing of 0.05 eV, and an energy cutoff of 500 eV. To obtain accurate electronic states, we set the energy tolerance to $10^{-5}$ eV and adopt dense k-meshes of $8 \times 8 \times 3$ for $n + m = 4$, $8 \times 8 \times 2$ for $n + m = 6$, and $8 \times 8 \times 1$ for $n + m = 8$ and 10.

## References


1. Chen, Y. Z. *et al.* A High-Mobility Two-Dimensional Electron Gas at the Spinel/Perovskite Interface of $\gamma$-$Al_2O_3/SrTiO_3$. *Nat. commun.* **4,** 1371 (2013).
2. Tojo, Y., Matoba, M. & Kamihara, Y. Annealing Induced Superconductivity in Perovskite-Related Iron-Based Mixed Anion Compounds $Sr_2VFeAsO_{3-x}$. *J. Appl. Phys.* **113,** 17E157 (2013).
3. Bahoosh, S. G. & Wesselinowa, J. M. The Origin of Magnetism in Perovskite Ferroelectric $ABO_3$ Nanoparticles (A = K,Li; B = Ta,Nb or A = Ba,Sr,Pb; B = Ti). *J. Appl. Phys.* **112,** 053907 (2012).
4. Kida, T. *et al.* High-Field Magnetization and Magnetoresistance of the A-site Ordered Perovskite Oxide $CaCu_3Ti_{4-x}Ru_xO_{12}$ ($0 \leq x \leq 4$). *Phys. Rev. B* **85,** 195122 (2012).
5. Cui, B. *et al.* Strain Engineering Induced Interfacial Self-Assembly and Intrinsic Exchange Bias in a Manganite Perovskite Film. *Sci. Rep.* **3,** 2542 (2013).
6. Guo, Y. Q. *et al.* Tunable Exchange Bias Effect in Sr-Doped Double Perovskite $La_2NiMnO_6$. *J. Phys. D: Appl. Phys.* **46,** 175302 (2013).
7. Wei, J. Y. T., Yeh, N. C., Vasquez, R. P. & Gupta, A. Tunneling Evidence of Half-metallicity in Epitaxial Films of Ferromagnetic Perovskite Manganites and Ferrimagnetic Magnetite. *J. Appl. Phys.* **83,** 7366–7368 (1998).
8. Nuraje, N. & Su, K. Perovskite Ferroelectric Nanomaterials. *Nanoscale* **5,** 8752–8780 (2013).
9. Dagotto, E. Complexity in Strongly Correlated Electronic Systems. *Science* **309,** 257–262 (2005).
10. Pesquera, D. *et al.* Surface Symmetry-Breaking and Strain Effects on Orbital Occupancy in Transition Metal Perovskite Epitaxial Films. *Nat. Commun.* **3,** 1189 (2010).
11. Nanda, B. R. K. & Satpathy, S. Electronic and Magnetic Structure of the $(LaMnO_3)_{2n}/(SrMnO_3)_n$ Superlattices. *Phys. Rev. B* **79,** 054428 (2009).
12. Narkilahti, J., Plekh, M., Levoska, J. & Tyunina, M. Anomalous Growth and Properties of $SrTiO_3$-$NaNbO_3$ Superlattices. *Phys. Rev. B* **79,** 014106 (2009).
13. Oja, R. & Nieminen, R. M. Modeling Charge-Imbalanced $NaNbO_3/SrTiO_3$ Superlattices: Lattice Relaxation and Metallicity. *Phys. Rev. B* **80,** 205420 (2009).
14. Lee, Y. *et al.* Phase Diagram of Electrostatically Doped $SrTiO_3$. *Phys. Rev. Lett.* **106,** 136809 (2011).
15. Ueno, K. *et al.* Effective Thickness of Two-Dimensional Superconductivity in a Tunable Triangular Quantum Well of $SrTiO_3$. *Phys. Rev. B* **89,** 020508(R) (2014).
16. Jin, S. *et al.* Thousandfold Change in Resistivity in Magnetoresistive La-Ca-Mn-O Films. *Science* **264,** 413–415 (1994).
17. Varela, M. *et al.* Atomic-Resolution Imaging of Oxidation States in Manganites. *Phys. Rev. B* **79,** 085117 (2009).
18. De, K. *et al.* Enhanced Ferromagnetism and Glassy State in Phase Separated $La_{0.95}Sr_{0.05}MnO_{3+x}$. *J. Appl. Phys.* **112,** 103907 (2012).
19. Demeter, M. *et al.* Electronic Structure of Doped La-Mn-O Perovskites. *Acta Phys. Pol. A* **98,** 587–591 (2000).
20. Choi, W. S. *et al.* Charge States and Magnetic Ordering in $LaMnO_3/SrTiO_3$ Superlattices. *Phys. Rev. B* **83,** 195113 (2011).
21. Yamada, H., Kawasaki, M., Lottermoser, T., Arima, T. & Tokura, Y. $LaMnO_3/SrMnO_3$ Interfaces with Coupled Charge-Spin-Orbital Modulation. *Appl. Phys. Lett.* **89,** 052506 (2006).
22. Bruno, F. Y. *et al.* Electronic and Magnetic Reconstructions in $La_{0.7}Sr_{0.3}MnO_3/SrTiO_3$ Heterostructures: A Case of Enhanced Interlayer Coupling Controlled by the Interface. *Phys. Rev. Lett.* **106,** 147205 (2011).
23. Barriocanal, J. G. *et al.* Charge Leakage at $LaMnO_3/SrTiO_3$ Interfaces. *Adv. Mater.* **22,** 627–632 (2010).
24. Kresse, G. & Joubert, D. From Ultrasoft Pseudopotentials to the Projector Augmented-Wave Method. *Phys. Rev. B* **59,** 1758–1775 (1999).
25. Blöchl, P. E., Jepsen, O. & Andersen, O. K. Improved Tetrahedron Method for Brillouin-Zone Integrations. *Phys. Rev. B* **49,** 16223–16233 (1994).
26. Lichtenstein, A. I. Density-Functional Theory and Strong Interactions: Orbital Ordering in Mott-Hubbard Insulators. *Phys. Rev. B* **52,** R5467–R5470 (1995).
27. Okatov, S., Poteryaev, A. & Lichtenstein, A. Structural Distortions and Orbital Ordering in $LaTiO_3$ and $YTiO_3$. *Europhys. Lett.* **70,** 499–505 (2005).
28. Okamoto, S., Millis, A. J. & Spaldin, N. A. Lattice Relaxation in Oxide Heterostructures: $LaTiO_3/SrTiO_3$ Superlattices. *Phys. Rev. Lett.* **97,** 056802 (2006).
29. Ma, C., Yang, Z. & Picozzi, S. Ab-initio Electronic and Magnetic Structure in $La_{0.66}Sr_{0.33}MnO_3$: Strain and Correlation Effects. *J. Phys.: Condens. Matter.* **18,** 7717–7728 (2006).
30. Tikhomirov, O., Jiang, H. & Levy, J. Local Ferroelectricity in $SrTiO_3$ Thin Films. *Phys. Rev. Lett.* **89,** 147601 (2002).
31. Liu, H. M., Ma, C. Y., Zhou, P. X., Dong, S. & Liu, J. M. Magnetic Orders and Electronic Structure in $LaMnO_3/SrTiO_3$ Superlattices. *J. Appl. Phys.* **113,** 17D902 (2013).
32. Zhong, W. & Vanderbilt, D. Effect of Quantum Fluctuations on Structural Phase Transitions in $SrTiO_3$ and $BaTiO_3$. *Phys. Rev. B* **53,** 5047–5050 (1996).
33. Goodenough, J. B. Theory of the Role of Covalence in the Perovskite-type Manganites [La, M(II)]$MnO_3$. *Phys. Rev.* **100,** 564–573 (1955).
34. Lee, J. S. *et al.* Titanium $d_{xy}$ Ferromagnetism at the $LaAlO_3/SrTiO_3$ Interface. *Nat. Mater.* **12,** 703–706 (2013).
35. Cossu, F., Singh, N. & Schwingenschlögl, U. High Mobility Half-metallicity in the $(LaMnO_3)_2/(SrTiO_3)_8$ Superlattice. *Appl. Phys. Lett.* **102,** 042401 (2013).
36. Grutter, A. J. *et al.* Interfacial Ferromagnetism in $LaNiO_3/CaMnO_3$ Superlattices. *Phys. Rev. Lett.* **111,** 087202 (2013).

37. Salluzzo, M. *et al.* Origin of Interface Magnetism in $BiMnO_3/SrTiO_3$ and $LaAlO_3/SrTiO_3$ Heterostructures. *Phys. Rev. Lett.* **111,** 087204 (2013).
38. Nanda, B. R. K. & Satpathy, S. Polar Catastrophe, Electron Leakage, and Magnetic Ordering at the $LaMnO_3/SrMnO_3$ Interface. *Phys. Rev. B* **81,** 224408 (2010).
39. Zener, C. Interaction Between the *d*-Shells in the Transition Metals. II. Ferromagnetic Compounds of Manganese with Perovskite Structure. *Phys. Rev.* **82,** 403–405 (1951).
40. Wollan, E. O. & Koehler, W. C. Neutron Diffraction Study of the Magnetic Properties of the Series of Perovskite-Type Compounds [(1-x)La, xCa]$MnO_3$, *Phys. Rev.* **100,** 545–563 (1955).
41. Pavlenko, N., Kopp, T., Tsymbal, E. Y., Sawatzky, G. A. & Mannhart, J. Magnetic and Superconducting Phases at the $LaAlO_3/SrTiO_3$ Interface: The Role of Interfacial Ti 3*d* Electrons. *Phys. Rev. B* **85,** 020407(R) (2012).
42. Santolino, G. S. *et al.* Oxygen Octahedral Distortions in $LaMnO_3/SrTiO_3$ Superlattices. *Microsc. Microanal.* **20,** 825–831 (2014).
43. Barriocanal, J. G. *et al.* Spin and Orbital Ti Magnetism at $LaMnO_3/SrTiO_3$ interfaces. *Nat. Commun.* **1,** 82 (2010).
44. Kalabukhov, A., Gunnarsson, R., Börjesson, J., Olsson, E., Claeson, T. & Winkler, D. Effect of Oxygen Vacancies in the $SrTiO_3$ Substrate on the Electrical Properties of the $LaAlO_3/SrTiO_3$ Interface. *Phys. Rev. B* **75,** 121404(R) (2007).
45. Takizawa, M. *et al.* Photoemission from Buried Interfaces in $SrTiO_3/LaTiO_3$ Superlattices. *Phys. Rev. Lett.* **97,** 057601 (2006).

## Acknowledgments

Research reported in this publication was supported by the King Abdullah University of Science and Technology (KAUST).

## Author Contributions

F.C. and U.S. designed the study. J.J. performed the calculations. All authors contributed to the interpretation of the results and the writing of the manuscript.

## Additional Information

**Supplementary information** accompanies this paper at http://www.nature.com/srep

**Competing financial interests:** The authors declare no competing financial interests.

**How to cite this article**: Jilili, J. *et al.* Trends in $(LaMnO_3)n/(SrTiO_3)m$ superlattices with varying layer thicknesses. *Sci. Rep.* **5**, 13762; doi: 10.1038/srep13762 (2015).